CHAPTER III
RESULTS AND DISCUSSION

3.1 Characterization of Polyaniline and the Doped Polyaniline Films

3.1.1 FTIR spectrophotometer

FTIR result of the synthesized polyaniline is shown in Figure 3.1. The important FTIR characteristic peaks of the synthesized polyaniline occur at the same positions as reported by Levon *et al.* (1995). All the peak locations, related to the chemical bonds, are tabulated in Table 3.1.
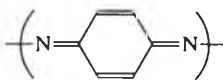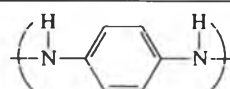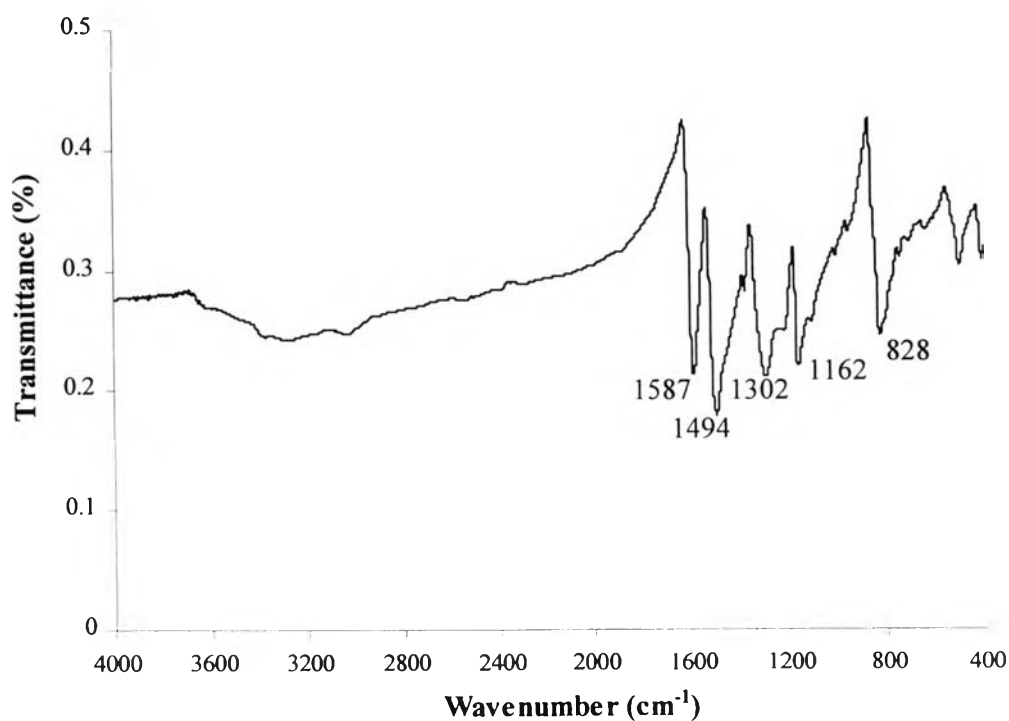

Figure 3.1 FTIR spectra of the undoped synthesized polyaniline (powder).

Table 3.1 The summarizing of FTIR characteristic peaks of the synthesized polyaniline.

Peaks location (cm^{-1})	Functional group
3264	N-H stretching of aromatic amine
3025	C-H stretching of aromatic hydrocarbon
1587	C=C stretching of quinoid imine
1494	C=C stretching of benzenoid diamine
1302	C-N-C stretching of a secondary of aromatic amine for both quinoid and benzenoid segments
1162	Vibration mode of quinoid segments
828	Out of plane bending of para-substitute of aromatic benzene ring

The absorption at 828 cm^{-1} indicates the type of substituted benzene in polyaniline. Other peaks indicating other types of substituted benzene are not observed. Therefore, the FTIR spectrum gives an evidence for the formation of poly(p-aniline) which is a polyaniline emeraldine base. Narayana *et al.* (1994) reported that the absorption at 1162 cm^{-1} indicates an electronic band which is associated with electrical conductivity in polyaniline. Kang *et al.* (1990) reported that the electronic band absorption at 1145 cm^{-1} becomes broader gradually upon increasing the organic acceptors in the doping process.

In the doped polyaniline films, the new absorption at 1664 cm^{-1} appears and can be attributed to the absorption of carbonyl group from the remaining NMP solvent and is shown in Figure 3.2. The changes in the

intensity ratio of the absorption peaks at 1594 and 1499 cm^{-1} are an evidence for the protonation doping process. The absorption at 1162 cm^{-1} in the synthesized polyaniline shifts to 1166-1135 cm^{-1} in the doped polyaniline. This indicates that the increase in planarity of the doped polyaniline films from the change in the conformation after the doping process. The electronic band absorption in the range 1166-1135 cm^{-1} of the doped films of (a), (b), (c), (d), (e) and (g) become broader at high ratios of C_a/C_p due to the high protonation level. All the absorption peaks of the doped films of samples (h) and (i) can not be seen clearly because of the increase in the electron delocalization along the polymer chains resulting from the high protonation level in doping process.
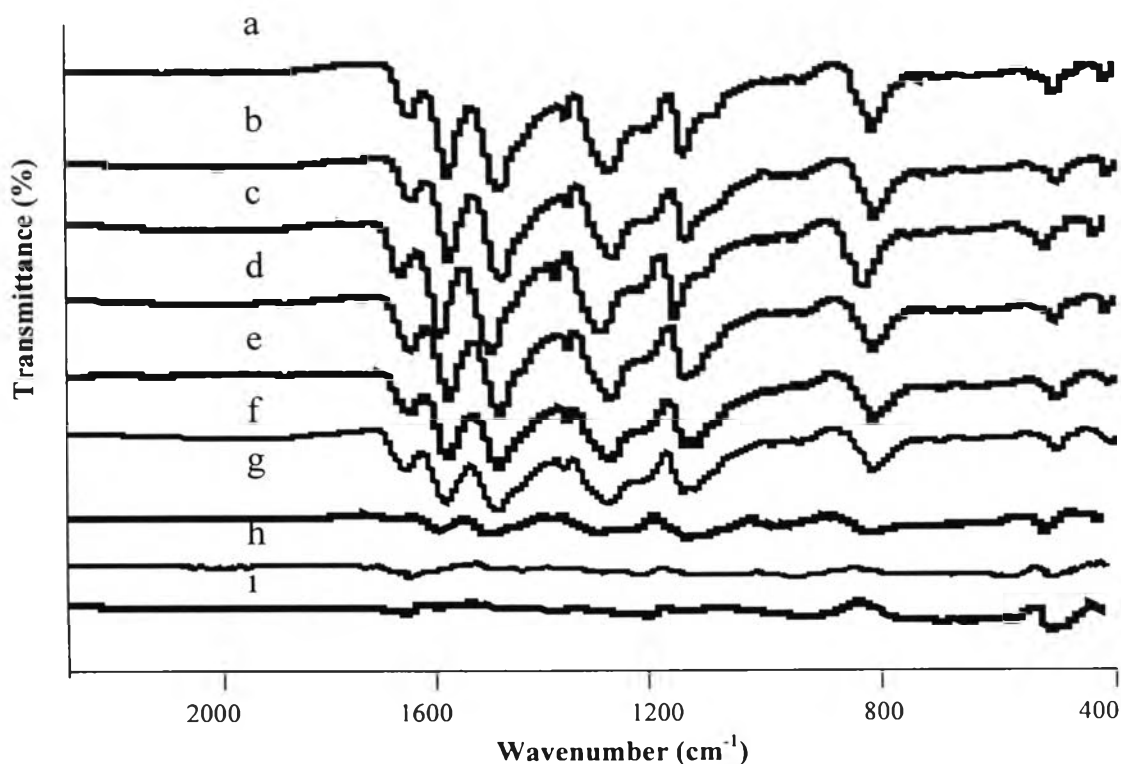

Figure 3.2 FTIR spectra of doped polyaniline films at various C_a/C_p : (a) 0, (b) 0.73, (c) 1.46, (d) 4, (e) 7.3, (f) 10.2, (g) 14.6, (h) 30 and (i) 50.

3.1.2 UV-visible spectrophotometer

The optical properties of conductive polymer play an important role in changing molecular conformation which can affect the electrical properties of conductive polymer. Figure 3.3 shows the UV-visible spectra of the solution of the synthesized polyaniline emraldine base in NMP solvent. The absorption at 343 nm indicates the $\pi-\pi^*$ transition electrons of the benzene ring delocalized onto nitrogen atoms of the amine in the benzenoid segments. The absorption at 655 nm indicates the excitation from the highest occupied molecular orbital (HOMO π_b) of the benzenoid ring to the lowest unoccupied molecular orbital (LUMO π_q) of the localized quinoid segments. The positions of the peak at 343 and 655 nm depend on the purification method and the level of purification of the synthesis.
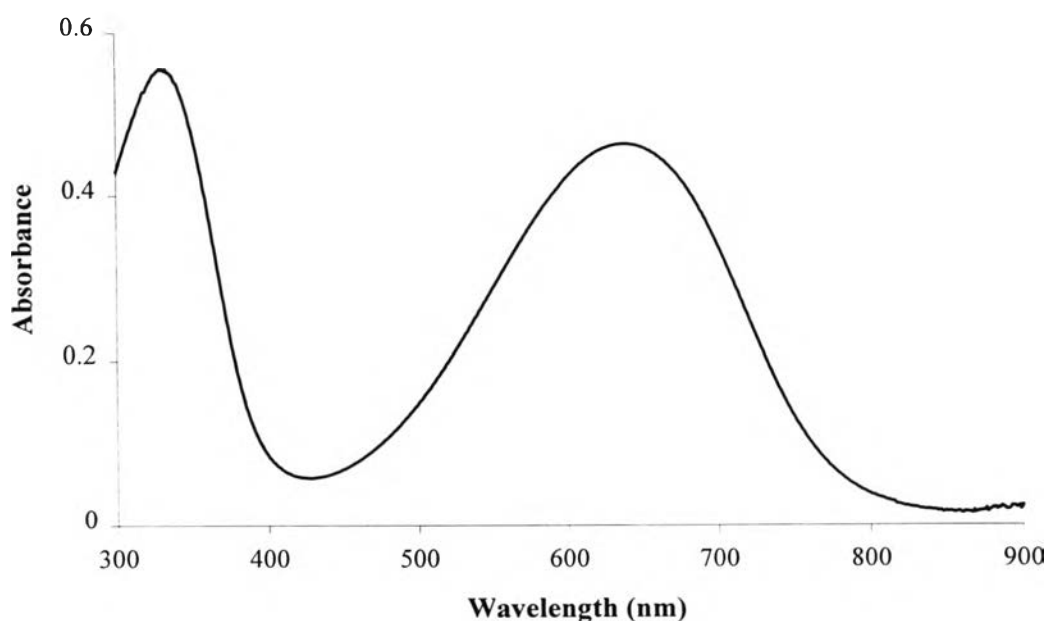

Figure 3.3 UV-visible spectra of the synthesized polyaniline solution in NMP.

Laakso *et al.* (1994) reported that pure polyaniline emeraldine base has two absorption peaks at approximately 325 and 605 nm. The absorption at 325 nm suggests the excitation of the benzene segment including amine structures in polyaniline. The peak at 605 nm indicates the quinoid structure including imines.

Figure 3.4 shows the UV-vis spectra of the undoped and doped polyaniline in the solutions at various ratios of C_a/C_p. These spectra show that the absorption at 665 nm for the doped polyaniline, C_a/C_p 0, 0.73, 1.46 and 4, gradually decreases with the increase in acid concentration. This indicates the progressive protonation at quinoid segments of polyaniline. In the sample of C_a/C_p equal to 7.3 and 10.2, the peak at 665 shifts to 527-540 nm because of the changes in molecular conformation at high protonation levels. The absorption at 665 and 540 nm disappear at the samples of C_a/C_p equal to 14.6, 30 and 50. The new peaks occur at 456 and 730 nm, identifying the transition of polaron state to π^* and the excitation of polaron state of the doped polyaniline respectively.
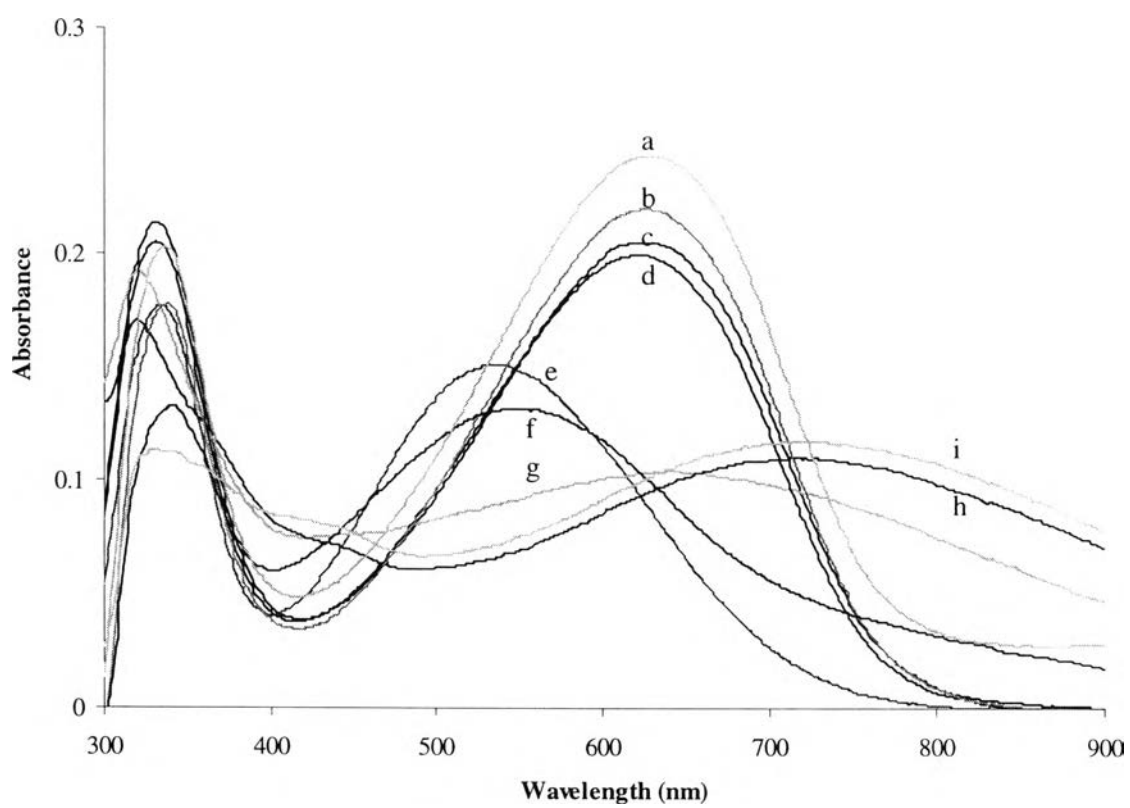
Figure 3.4 UV-visible spectra of the doped polyaniline solution in NMP solvent at various C_a/C_p : (a) 0, (b) 0.73, (c) 1.46, (d) 4, (e) 7.3, (f) 10.2, (g) 14.6, (h) 30 and (i) 50.

Figure 3.5 shows the result of UV-visible measurement of the doped polyaniline films at different acid concentrations. This result shows that the intensity of the absorption at 655 nm for sample, $C_a/C_p = 0$, gradually decreases from samples (a) to (f) in the order of increasing acid concentration due to the higher protonation levels at nitrogen atoms in quinoid segments. The molecular structure of quinoid sites changes to partially protonated structure is demonstrated in Table 1.2. At the highest acid concentration, $C_a/C_p = 50$, the absorption at 650 nm disappears and new absorption at 448 and 870 nm occur due to the change in quinoid segments to the positive radical of the polaron state in polyaniline emeraldine salt. The absorptions at 448 and 870 nm indicate the transition of polaron state to π^* and the polaron state of the doped polyaniline respectively. In the case of samples (g) and (h), there are no well-defined peaks because of the change in quinoid site to some polaron and bipolaron states.
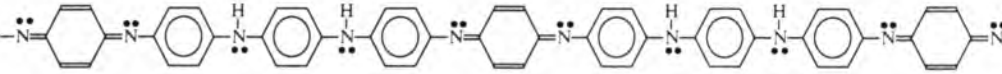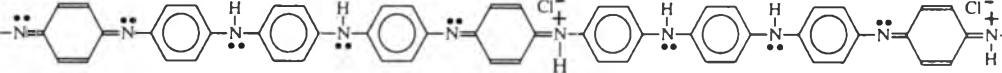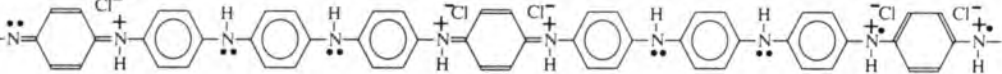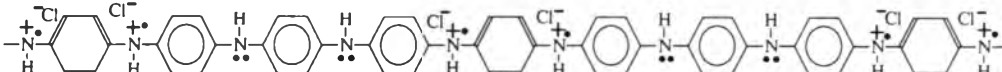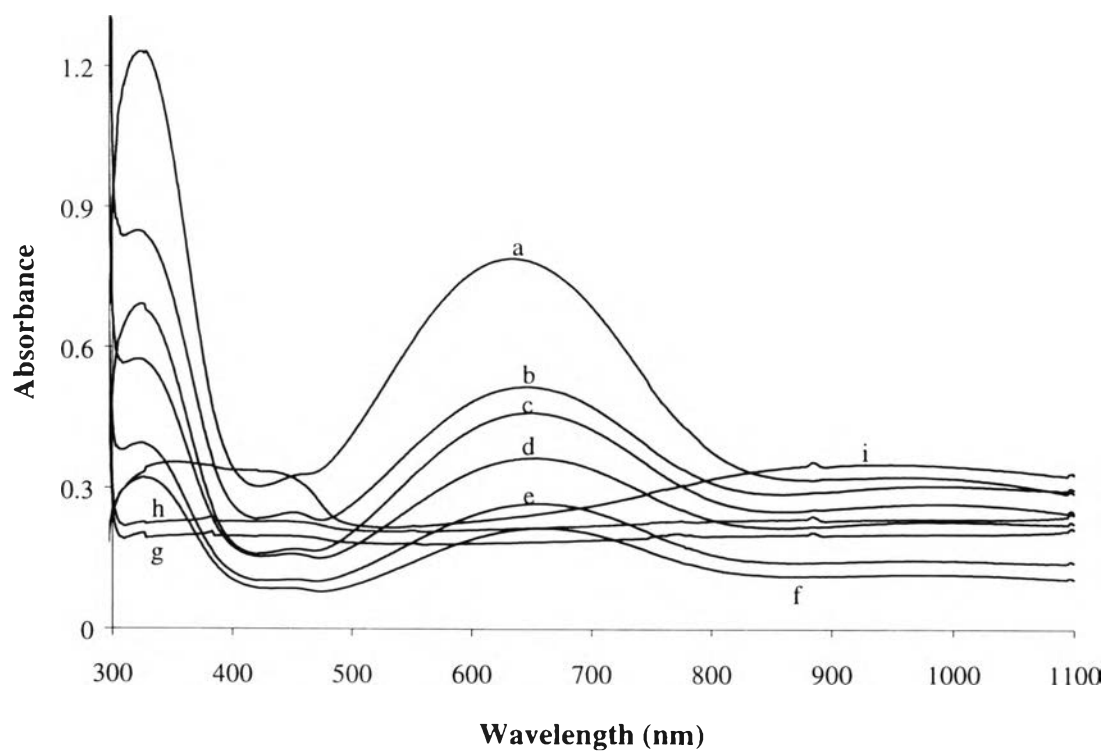
Figure 3.5 UV-visible spectrum of the doped polyaniline films at various C_a/C_p : (a) 0, (b) 0.73, (c) 1.46, (d) 4, (e) 7.3, (f) 10.2, (g) 14.6, (h) 30 and (i) 50.

Table 3.2 The proposed structures of the doped polyaniline film at different acid concentrations.

C_a/C_p	Absorbance	Structures
(a) $C_a/C_p = 0$	337 nm: $\pi-\pi^*$ of benzenoid 646 nm: $\pi-\pi^*$ of quinoid	Polyaniline Emeraldine Base Bezenoid Quinoid
(b)$C_a/C_p= 0.73$	337 nm: $\pi-\pi^*$ of benzenoid 658 nm: $\pi-\pi^*$ of quinoid and some protonation	
(h)$C_a/C_p = 30$	No well defined peaks	 Bipolaron Polaron
(i)$C_a/C_p = 50$	477 nm: transition of polaron to π^* 890 nm: polaron	Polyaniline Emeraldine Salt Polaron

3.1.3 Elemental Analysis (EA)

In the protonation doping process of polyaniline, the amount of protons from hydrochloric acid protonated at nitrogen atoms in the polymer chain was determined in terms of doping level. The doping level of the doped films at various C_a/C_p ratios were monitored by the determination of carbon (C), hydrogen (H) and nitrogen (N) atoms from elemental analysis. The doping levels were calculated from Equation 2.2.
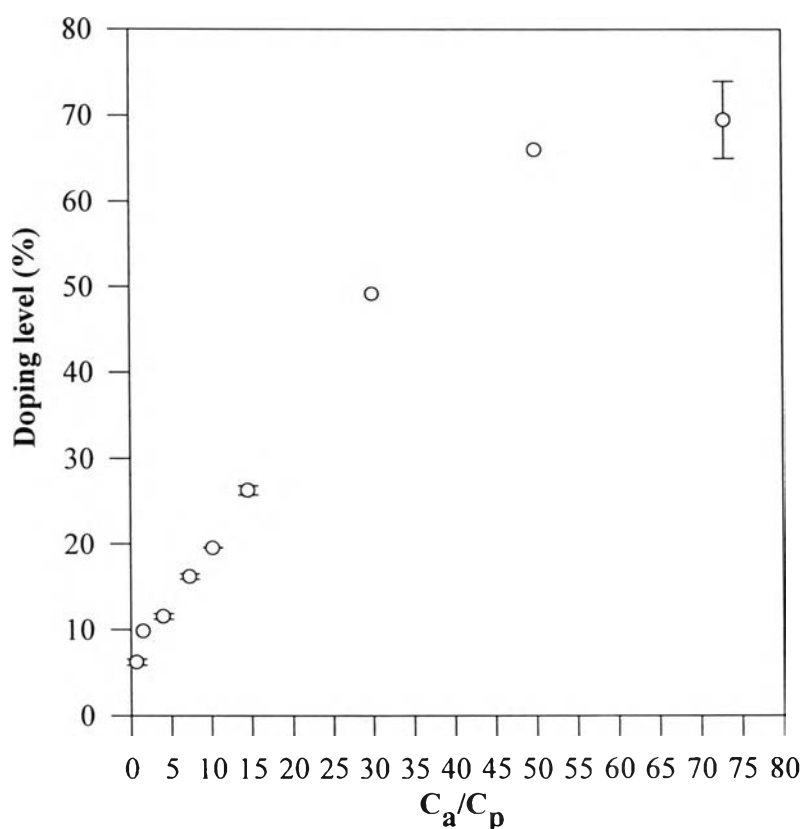

Figure 3.6 The percentage of doping level as a function of C_a/C_p of the doped films at C_a/C_p: (a) 0, (b) 0.73, (c) 1.46, (d) 4, (e) 7.3, (f) 10.2, (g) 14.6, (h) 30 and (i) 50.

The result of EA measurement is shown in Figure 3.6. This graph shows that the doping level sharply increases with the ratio of C_a/C_p from 0.7 to 50. This indicates that the doped polyaniline is gradually protonated with acid concentration. The doping level becomes constant at C_a/C_p equal to 50 due to the saturated protonation at the nitrogen atoms in polyaniline.

The empirical formula of the chemical structure of the doped polyaniline at different acid concentrations can also calculated from the data of elemental analysis and are shown in Table 3.3.

Table 3.3 Mole ratio normalized to nitrogen atom of the doped polyaniline films.

| C_a/C_p	Chemical Structures Normalized to N atom		
	C	H	N
0.73	6.26	5.21	1
1.46	6.24	5.49	1
4	6.17	5.51	1
7.3	6.16	5.48	1
10.2	6.12	5.61	1
14.6	6.13	5.70	1
30	6.27	6.31	1
50	5.57	6.44	1
73	5.44	6.88	1

3.1.4 Scanning Electron Microscope (SEM)

The doped polyaniline in the forms of powder and film were studied to identify and to understand the relations between microstructures and electrical properties. Figure 3.7 shows the result of SEM measurement of the doped polyaniline powder at different acid concentrations. This figure shows that the compact coil morphology is formed in the undoped polyaniline powder. When polyaniline powders are protonated with low concentration of hydrochloric acid as in the sample of (f), $C_a/C_p = 10.2$, the loose loop structures are observed. This is due to the partially protonation at nitrogen atoms and causes some repulsion between the positive charges. In the case of polyaniline powders which are protonated with high acid concentrations, $C_a/C_p = 50$, the doped polyaniline have an expanded structure due to the high repulsive force from the high positive charges in the chain. The proposed structures of the doped polyaniline powder are shown in Figure 3.8.
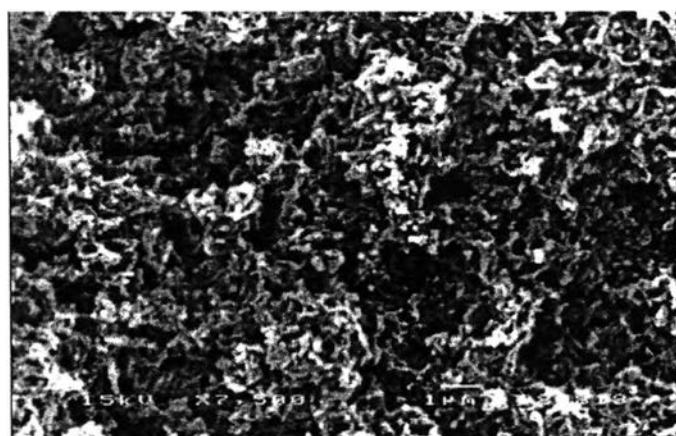
Chen *et al.* (1991) reported that the granular morphology was observed in the undoped polyaniline which was synthesized by chemical method. On the other hand, the electrochemical by synthesized undoped polyaniline had a fibrillar network morphology.
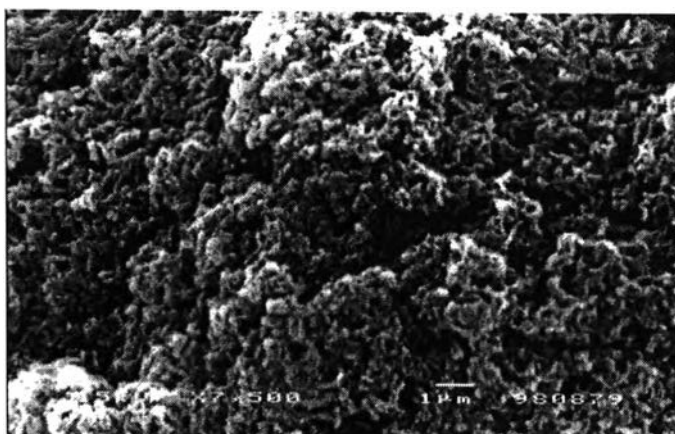
(a) $C_a/C_p = 0$
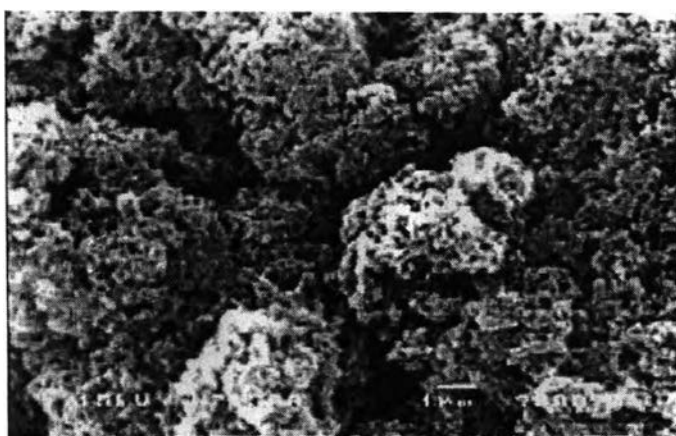
(f) $C_a/C_p = 10.2$

(i) $C_a/C_p = 50$

Figure 3.7 SEM micrographs of the doped polyaniline in the powder form at C_a/C_p equal to (a) 0, (f) 10.2 and (i) 50.
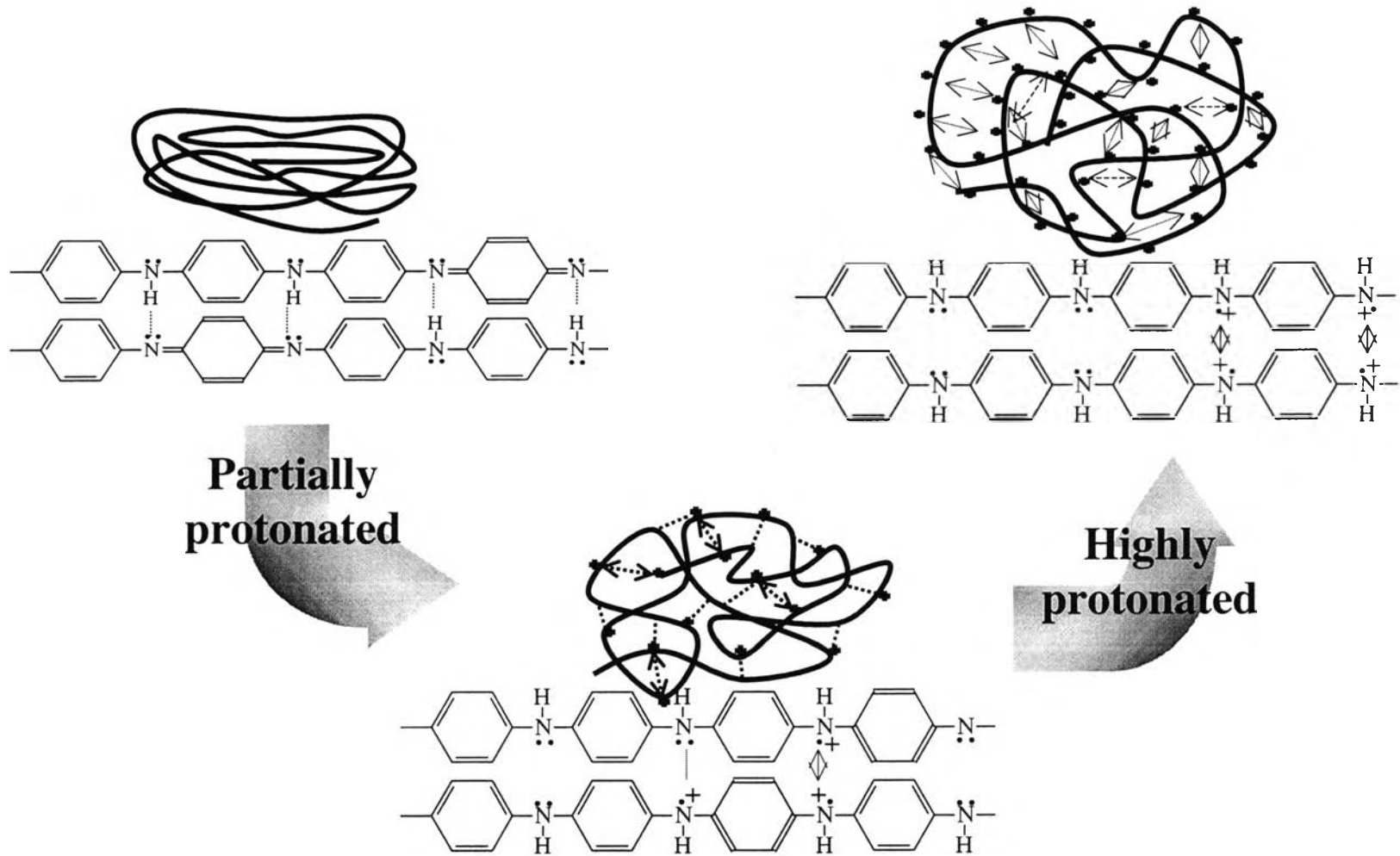
Figure 3.8 The proposed model of the doped polyaniline in the form of powder for morphology study.

3.1.5 Thermogravimetric Analysis (TGA)

Figure 3.9 shows the result of TGA measurement of the undoped and doped films at C_a/C_p of 0, 4 and 73. The TGA thermograms of these films show three steps weight loss behaviors. The first step; an initial weight loss (1.7 % for undoped film at $C_a/C_p = 0$, 2.55 and 2.63 % for doped films at $C_a/C_p = 4$ and 73) can be seen at temperature from 20-100°C. This is due to the evaporation of water from the polymer matrix as reported by Zilberman (1997). The possibility of the evaporation of HCl dopant can occur as well in this temperature range for the doped films. The second step; 8-9 % weight loss for both the undoped and doped films occur from 100-350°C. This weight loss is due to the evaporation of the remaining NMP solvent in the film and the loss of low molecular weight oligomers. For the last step, the undoped film shows the onset temperature at 457°C due to the decomposition of polymer backbone. The onset temperature of the doped film, 460-490°C, is higher than that of the undoped film due to the interchain and intrachain delocalizations.
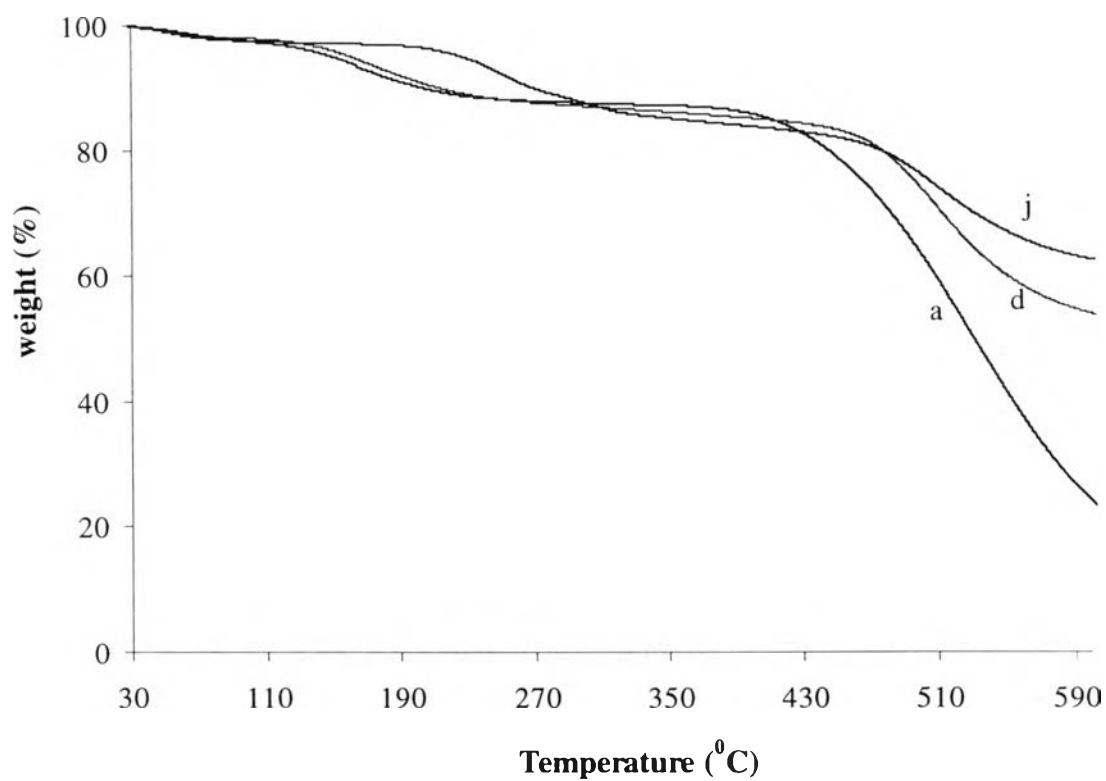
Figure 3.9 TGA thermogram of the undoped and doped film at C_a/C_p: (a) 0, (d) 4 and (j) 73.

3.2 Electrical Property of the Doped Polyaniline

      3.2.1 <u>Effect of Aging on the electrical conductivity of the doped</u> <u>polyaniline</u>

Effect of aging on the electrical conductivity of the doped polyaniline films at different ratios of C_a/C_p is shown in Figure 3.10. This graph shows that the electrical conductivity of the doped film at C_a/C_p equal to 14.6 sharply decreases during the period of 1 to 20 days. For the doped films at C_a/C_p equal to 50 and 73, the electrical conductivities of these films gradually decrease during the period of 1 to 20 days. The oxidation from oxygen in air causes the decrease in the electrical conductivity of these doped films. Oxygen molecules can absorb onto the surface of the doped films and diffuse into the interior to oxidize the nitrogen atoms. The oxidation process enlarges the intermolecular distance between the neighboring polyaniline chains due to the high repulsion from the positive nitrogen atoms. This suggests that the doped polyaniline chains are aligned in the disorder form within the metallic-conducting region. The disordered chains in the metallic region cause a reduction of the interchain electron diffusion rate. Therefore a decrease in electrical conductivity occurs during a period of 20 days. The oxidation process also reduces the localization lengths of the doped polyanilines. This means that the electrons in polaron state of the doped polyaniline are delocalized in a shorter and limited localization length, causing the decrease in electrical conductivity.

Dalas *et al* (1998) reported that the decrease in the electrical conductivity of polyaniline and polypyrrole can be attributed to the oxidation of air. Oxygen gas can diffuse into doped polyaniline films and disrupt the conduction pathway.

Park *et at* (1998) reported that the conductivities of the copolymeric acids-doped polyaniline decrease as the content of the nonacidic

units in the acid dopants increase. Steric effect of the nonacid units causes the interchain seperation of polyaniline chain to decrease the interchain electron diffusion rate.
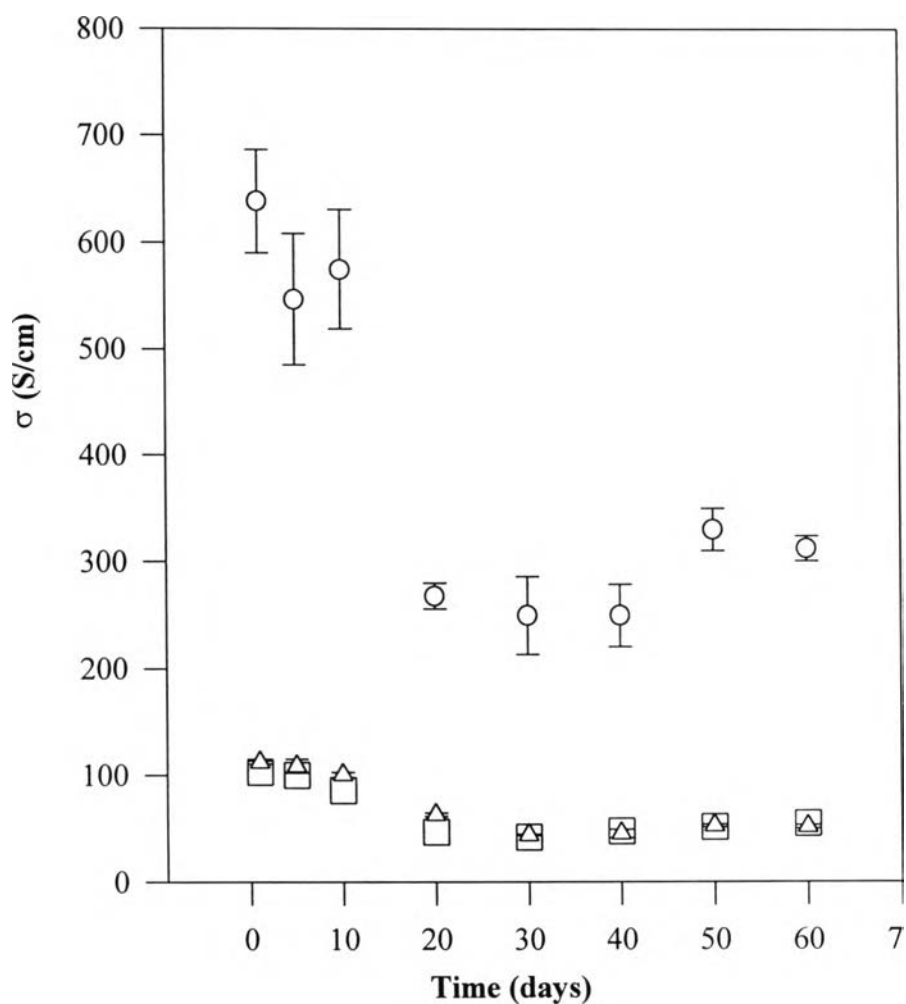

Figure 3.10 The electrical conductivity (σ) of the doped polyaniline film as a function of time (days) at various C_a/C_p : (g) 14.6,$\bigcirc$, (i) 50,$\triangle$ and (j) 73,$\square$.

3.2.2 <u>Effect of Acid Concentration on the conductivity of the doped</u>
<u>polyaniline films</u>

Effect of acid concentration on the electrical conductivity of the doped polyaniline films at different ratios of C_a/C_p is shown in Figure 3.11. This graph shows that the electrical conductivity sharply increase for the doped films whose C_a/C_p are equal to 7.3 to 30 due to increasing protonation levels. The maximum electrical conductivity occurs for the doped films at C_a/C_p equal to 14.6 and 30 due to the delocalization of the electrons in the interchain and intrachain directions at the equilibrium protonation level of the doped film. Beyond the doped film at C_a/C_p equal to 30, the electrical conductivity sharply decreases. When polyaniline films are protonated with excess acid concentration, positive charges at nitrogen atoms cause the reduction in the delocalization length in the polymer chain. Therefore the decrease in the electrical conductivity occurs at the higher ratios of C_a/C_p. The proposed model for explanation the electrical conductivity of the doped films as a function of acid concentration is shown in Figure 3.12.
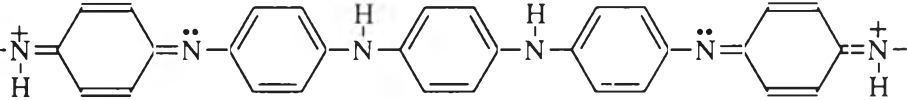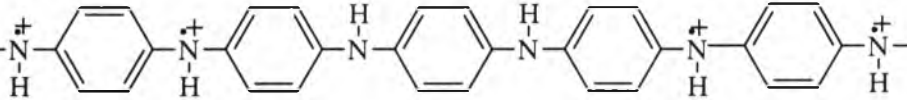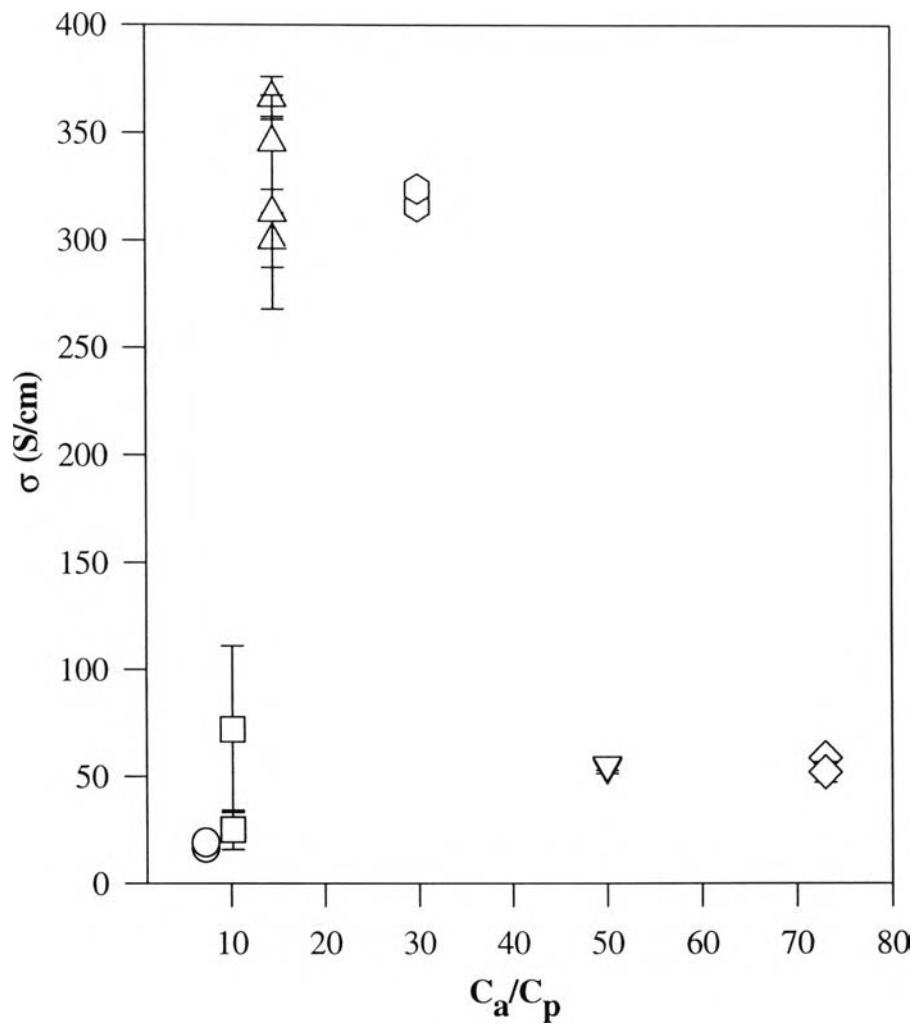
Figure 3.11 The electrical conductivity as a function of acid concentration of the doped films at C_a/C_p : (e) 7.3,$\bigcirc$, (f) 10.2, $\square$, (g) 14.6,$\triangle$, (h) 30, $\ominus$, (i) 50, ∇ , and (j) 73, $\diamondsuit$.

Table 3.4 The proposed structures of the doped polyaniline films as a function of acid concentrations.

C_a/C_p	Explanations	The proposed structures
(e) 7.3	-Some protonation at quinoid segments -Lower the electrical conductivity	
(g) 14.6	-Equilibrium protonation at quinoid segments -The delocalization of electrons in the interchain and intrachain directions -Maximum the electrical conductivity	
(j) 73	-Shorten delocalization lengths -Electron delocalization only in the shorten limited length in intrachain direction. -Lower the electrical conductivity	